CMS Draft Analysis Note

The content of this note is intended for CMS internal use and distribution only

Search for Dijet Resonances in the Dijet Mass Distribution in pp Collisions at $\sqrt{s} = 7\,\text{TeV}$

Robert M Harris[1], Ken Hatakeyama[6], Bora Isildak[4], Shabnam Jabeen[8], Chiyoung Jeong[3], Kostas Kousouris[1], Sung-Won Lee[3], Kalanand Mishra[1], Sertac Ozturk[2], Kai Yi[5], and Marek Zielinski[7]

[1] Fermilab, Batavia, IL, USA
[2] University of Cukurova, Adana, Turkey
[3] Texas Tech University, Lubbock, TX, USA
[4] Bogazici University, Istanbul, Turkey
[5] University of Iowa, Iowa City, IA, USA
[6] Baylor Univeristy, Baylor, TX, USA
[7] University of Rochester, Rochester, NY, USA
[8] Brown University, Providence, RI, USA

Abstract

INCOMPLETE AND VERY ROUGH DRAFT BASED ON 1 nb^{-1} OF DATA.

We present the first measurement of the dijet invariant mass spectrum and search for new particles decaying to dijets at CMS in pp collisions at $\sqrt{s} = 7$ TeV. The dijet mass distribution of the two leading jets in the pseudorapidity region $|\eta| < 1.3$ is measured and compared to QCD predictions from PYTHIA and the CMS detector simulation. We fit the observed dijet mass spectrum with a parameterization, search for dijet resonances, and set upper limits at 95% CL on the resonance cross section. These generic cross section limits are compared with theoretical predictions for the cross section for several models of new particles: axigluons, flavor universal colorons, excited quarks, E6 diquarks, Randall Sundrum Gravitons, W' and Z'.

1 Introduction

In this note we document our first measurement of the dijet mass distribution and our first search for dijet resonances in pp Collisions at $\sqrt{s} = 7$ TeV. The note is also intended as documentation for a Physics Analysis Summary document for approved CMS results for the ICHEP conference in July 2010. This is a very rough and incomplete draft based on 1 nb^{-1} of data. Please also see previous documents on simulation of the complete analysis in [1] and [2].

1.1 Motivation

Our experimental motivation is to make a first measurement of the dijet mass distribution and see whether it agrees with expectations or contains new physics beyond the Standard Model (SM). The LHC is a parton-parton collider in a previously unexplored energy region. If new parton-parton resonances exist at sufficiently low mass then the LHC will produce them copiously. These resonances must also decay to partons giving two jets in the final state. One theoretical motivation is that the SM has important unanswered questions. Why do quarks come in different flavors? Why are the quarks arranged in generations? Why are there four different forces? How do we unify gravitation with the other forces? Why is gravity so weak? Models that try to address these questions often predict short-lived particles that can decay to two partons: dijet resonances.

1.2 Models

We search for processes producing narrow resonances, X, decaying to dijets as illustrated in fig. 1: $pp \rightarrow X \rightarrow$ jet + jet (inclusive).
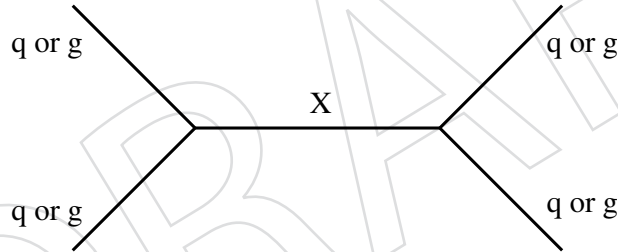

Figure 1: Feynman Diagram of dijet resonance. The initial state and final stat e both contain two partons (quarks, antiquarks or gluons) and the intermediate state contains a n s-channel resonance X.

We perform a generic search that we can apply to any model. Here we introduce some models in order of decreasing cross section at low mass, say a few words about the cross section, and explicitly list the partons involved in production and decay, as previously written [3]. Excited states of composite quarks [4] are strongly produced giving large cross sections ($qg \rightarrow q^*$). Axigluons [5] or colorons [6] from an additional color interaction are also strongly produced, but require an antiquark in the initial state ($q\bar{q} \rightarrow A$ or C) slightly reducing the cross section compared to excited quarks. Diquarks [7] from superstring inspired E_6 grand unified models are produced with electromagnetic coupling from the valence quarks of the proton ($ud \rightarrow D$). The cross section for E_6 diquarks at high mass is the largest of all the models considered, because at high parton momentum the probability of finding a quark in the proton is significantly larger than the probability of finding a gluon or antiquark. Randall Sundrum gravitons [8] from a model of large extra dimensions are produced from gluons or quark-antiquark pairs in the initial state ($q\bar{q}, gg \rightarrow G$). Heavy W bosons [9] inspired by left-right symmetric grand unified models have electroweak couplings and require antiquarks for their production($q_1\bar{q}_2 \rightarrow W'$),

giving small cross sections. Heavy Z bosons [9] inspired by grand-unified models are widely anticipated by theorists, but they are electroweakly produced, and require an antiquark in the initial state($q\bar{q} \rightarrow Z'$), so their production cross section is around the lowest of the models considered. Table 1 summarizes some properties of these models.

Model Name	X	Color	J^P	$\Gamma/(2M)$	Chan
Excited Quark	q*	Triplet	$1/2^+$	0.02	qg
E_6 Diquark	D	Triplet	0^+	0.004	qq
Axigluon	A	Octet	1^+	0.05	$q\bar{q}$
Coloron	C	Octet	1^-	0.05	$q\bar{q}$
RS Graviton	G	Singlet	2^-	0.01	$q\bar{q}$, gg
Heavy W	W'	Singlet	1^-	0.01	$q\bar{q}$
Heavy Z	Z'	Singlet	1^-	0.01	$q\bar{q}$

Table 1: Propserties of Some Resonance Models

Published lower limits [10] on the mass of these models in the dijet channel are listed in table 2.

q^*	A or C	D	ρ_{T8}	W'	Z'	G
0.87	1.25	0.63	1.1	0.84	0.74	-

Table 2: Published lower limits in TeV on the mass of new particles considered in this analysis. These 95% confidence level exclusions from the Tevatron [10] are the best published limits in the dijet channel.

1.3   Summary of Experimental Technique

QCD dijet events are the dominant process in a hadron collision. Our experimental method to search for dijet resonances utilizes the dijet mass spectrum measured in the data. If a resonance exists, it should appear in the dijet mass spectrum as a bump. First we compare the dijet mass spectrum to QCD predictions from PYTHIA to see if they agree. Next we fit the dijet mass spectrum with a smooth parameterization and see whether we can get a good fit. We look at the difference between the data and the fit, and estimate the significance of any bump in the data. If there is no significant evidence for dijet resonances, we proceed to set limits. The dijet resonance shape for generic di-parton resonances containing qq, qg and gg partons were simulated using PYTHIA as resonance signals. To calculate the upper cross section limit for this dijet resonance shape in our data, we perform a binned maximum likelihood method. The method gives a Poisson likelihood as a function of the cross section. We convolute the statistical likelihood distribution with our Gaussian systematic uncertainty and find the 95% confidence level upper limit on the cross section. This gives cross section limits for generic narrow qq, qg and gg resonances, independent of any specific resonance model. The upper limit on the cross section is then compared with the predicted cross section for a few models to obtain mass limits on particular models.

2   Measurement of Dijet Mass Spectrum

In this section we explain how we measure the dijet mass spectrum in data and compare it with Monte Carlo predictions.

2.1 Data Sample

Our collision dataset was

```
/MinimumBias/Commissioning10-PromptReco-v8/RECO (runs 132599-133510)
/MinimumBias/Commissioning10-PromptReco-v9/RECO (runs 133874-133887)
```

we run over this dataset at the Fermilab LPC and select the following good runs taken during April 1-24 2010:

```
132599,132601,132602,132605,132606,132646-132648,132650,132651,132653,
132654,132656,132658-132661,132716,132959-132961,132965,132966,132968,
133034,133036,133038,133046,133082,133158,133320,133321,133324,133446,
133448,133450,133474,133483,133509,133510,133874,133875,133876,133877,
133881,133885 and 133887.
```

We make the following Trigger bit selections for this minimum bias sample: 0 AND (40 OR 41) AND NOT (36 OR 37 OR 38 OR 39). We apply scraping event removal and a preselection that requires each event to have a jet with raw $p_T > 3$ GeV. This preselection job writes out root trees from the InclusiveJetTreeProducer on cmslpc.fnal.gov.

2.2 Jet Reconstruction

Jets are reconstructed using the Anti-KT algorithm with cone size $R = \sqrt{(\Delta\eta)^2 + (\Delta\phi)^2} = 0.7$. Below we will discuss three types of jets: reconstructed, corrected and generated. The reconstructed jet energy, E, is defined as the scalar sum of the calorimeter tower energies inside the jet. The jet momentum, $\vec{p}$, is the corresponding vector sum: $\vec{p} = \sum E_i \hat{u}_i$ with $\hat{u}_i$ being the unit vector pointing from the origin to the energy deposition E_i inside the cone. The jet transverse momentum, p_T, is the component of $\vec{p}$ in the transverse plane. The E and $\vec{p}$ of a reconstructed jet are then corrected for the non-linear response of the calorimeter to a generated jet. Generated jets come from applying the same jet algorithm to the Lorentz vectors of stable generated particles before detector simulation. The corrections are chosen so that, on average, the p_T of a corrected jet is equal to the p_T of the corresponding generated jet.

The corrections used for this analysis are the CMS standard relative (L2) and absolute(L3) jet corrections for η and p_T variation of the jet response using tag "Summer09_7TeV_ReReco332".

The dijet system is composed of the two jets with the highest p_T in an event (leading jets), and the dijet mass is given by $m = \sqrt{(E_1 + E_2)^2 - (\vec{p}_1 + \vec{p}_2)^2}$.

2.3 Event Selection

We run on the InclusiveJetRoot trees and produce a single processed root tree. In this step we select the Anti-KT 0.7 jets and apply the jet corrections. We also select the HLT_PhysicsDeclared bit and perform a dijet mass preselection of $m > 30$ GeV corrected. From the processed trees we perform the final analysis. We require there to be a good primary vertex with z value within 15 cms of the center of the detector and a number of degrees of freedom of at least 4.

Finally, we require both the leading jets to satisfy $|\eta| < 1.3$. This cut serves several purposes.

- It suppresses QCD processes significantly more than dijet resonances.
- It defines a fiducial region for our measurement predominantly in the Barrel.

100   • It provide a faster trigger turn on curve for the jet trigger which uses E_T, allowing
101   us to start the analysis at lower mass.

102 These cuts are used to make a histogram of dijet mass and other quantities (MassResults_ak7calo.root)
103 which is saved, along with the processed root tree (ProcessedTree_ak7calo.root) on cmslpc.fnal.gov
104 at

105 `/uscms_data/d2/kkousour/7TeV/DijetMassAnalysis/`

2.4   Dijet Mass Spectrum

107 The trigger efficiency, measured from a sample acquired with a prescaled trigger with a lower
108 p_T threshold, was greater than 99% for dijet mass above 137 GeV/c^2 as shown in Fig. 2. So, We
109 start the Dijet Mass Spectra from 137 GeV/c^2.
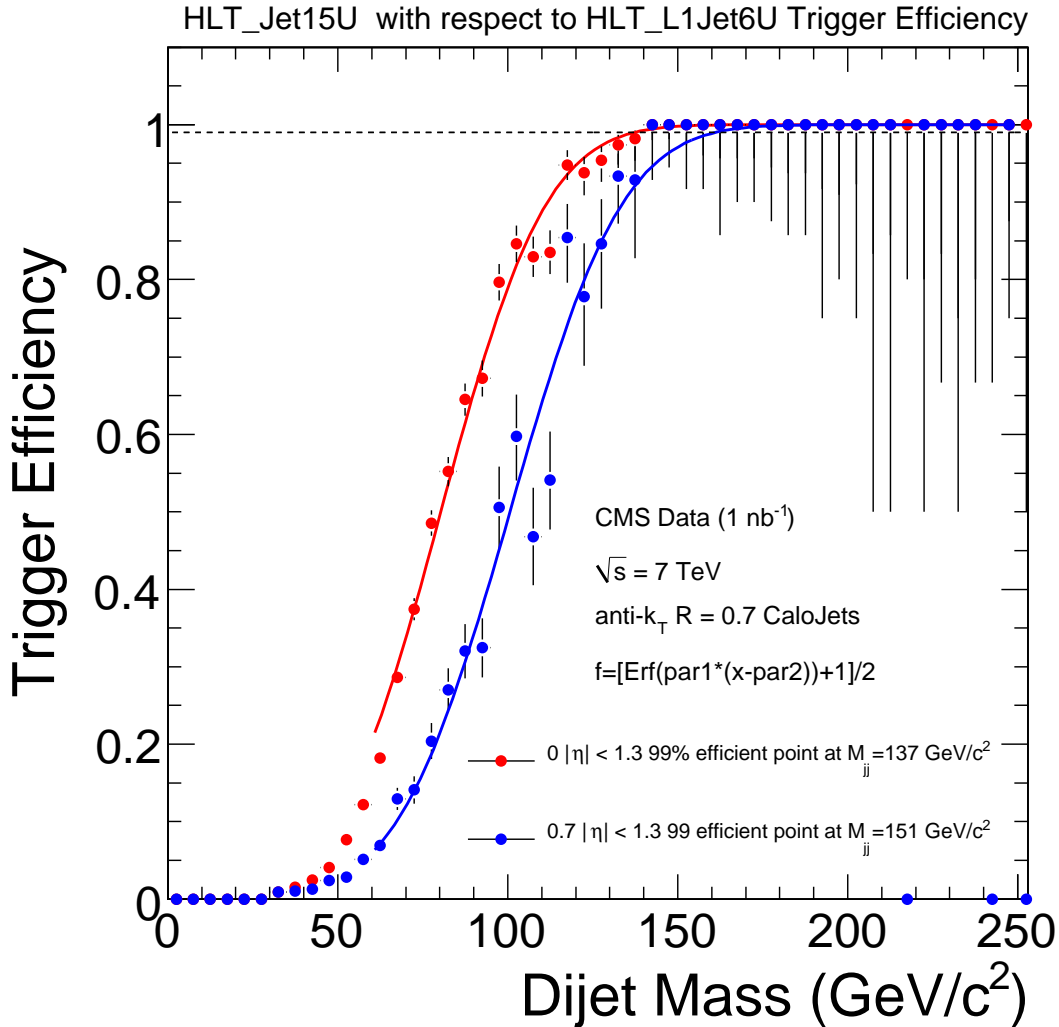
Figure 2: HLT_Jet15U trigger efficiency as a function of dijet mass, shown for two intervals of
pseudorapidity, one corresponding to this analysis ($|\eta| < 1.3$) and one that is important for the
dijet centrality ratio $0.7 < |\eta 1.3$.

110 We present some basic distributions indicating jet and event quality in Fig. 3. The basic distri-
111 butions look fine. The dijet events have low MET/ΣE_T indicating that the event energy is well

balanced in the transverse plane. EMF, the fraction of jet energy in the ECAL, is distributed smoothly for the two leading jets, with no peaks near either zero or one which would indicate a problem from the HCAL or ECAL. The two leading jets are back-to-back in ϕ as expected for dijets. The η - ϕ distribution of two leading jets is uniform and does not show any indication of hot or dead regions of the calorimeter.
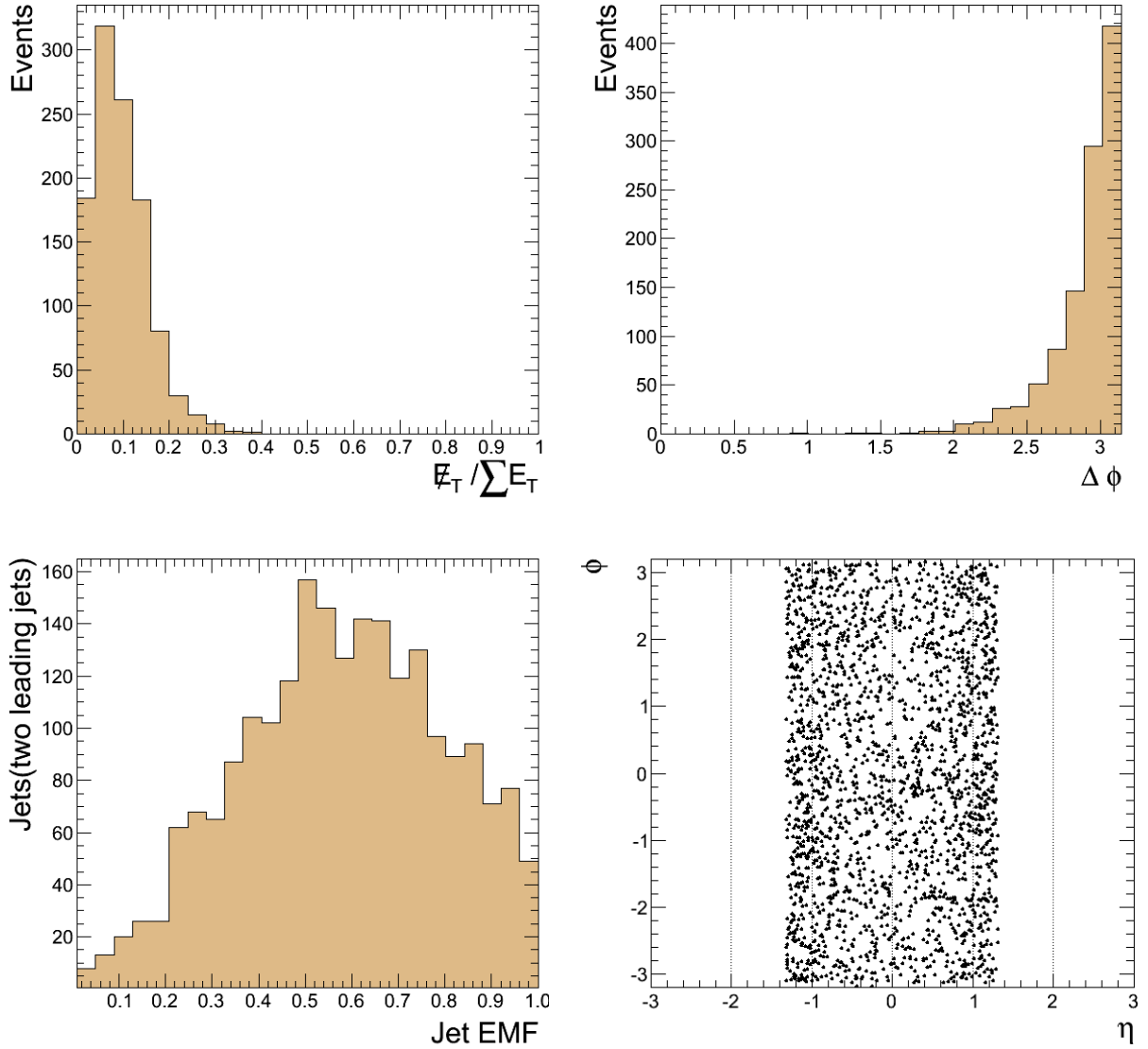

Figure 3: Basic Event and Jet Quality Distributions. upper left) Missing calorimeter E_T divided by total calorimeter E_T. upper right) The phi difference of the two leading jets. lower left) The EM energy fraction of the two leading jets. lower right) Jet ϕ vs. η for the two leading jets.

117 The measured dijet mass spectrum is shown in Fig 4. The mass spectrum is defined by

$$\frac{dN}{dm} = \frac{N_i}{\Delta m_i} \tag{1}$$

118 where m is the dijet mass, N_i is the number of events in the i-th dijet mass bin, and Δm_i is
119 the width of the i-th dijet mass bin. The bin width is approximately the dijet mass resolution,
120 and gradually increases as a function of mass. The data is compared to a PYTHIA QCD MC
121 prediction that has been normalized to have the same number of events as the data in this plot.
122 This normalization of the MC is the same as multiplying the absolute normalization prediction
123 for this luminosity by a factor of 0.82. The shape of the PYTHIA QCD MC prediction is close
124 to the data and there is no evidence for new physics.
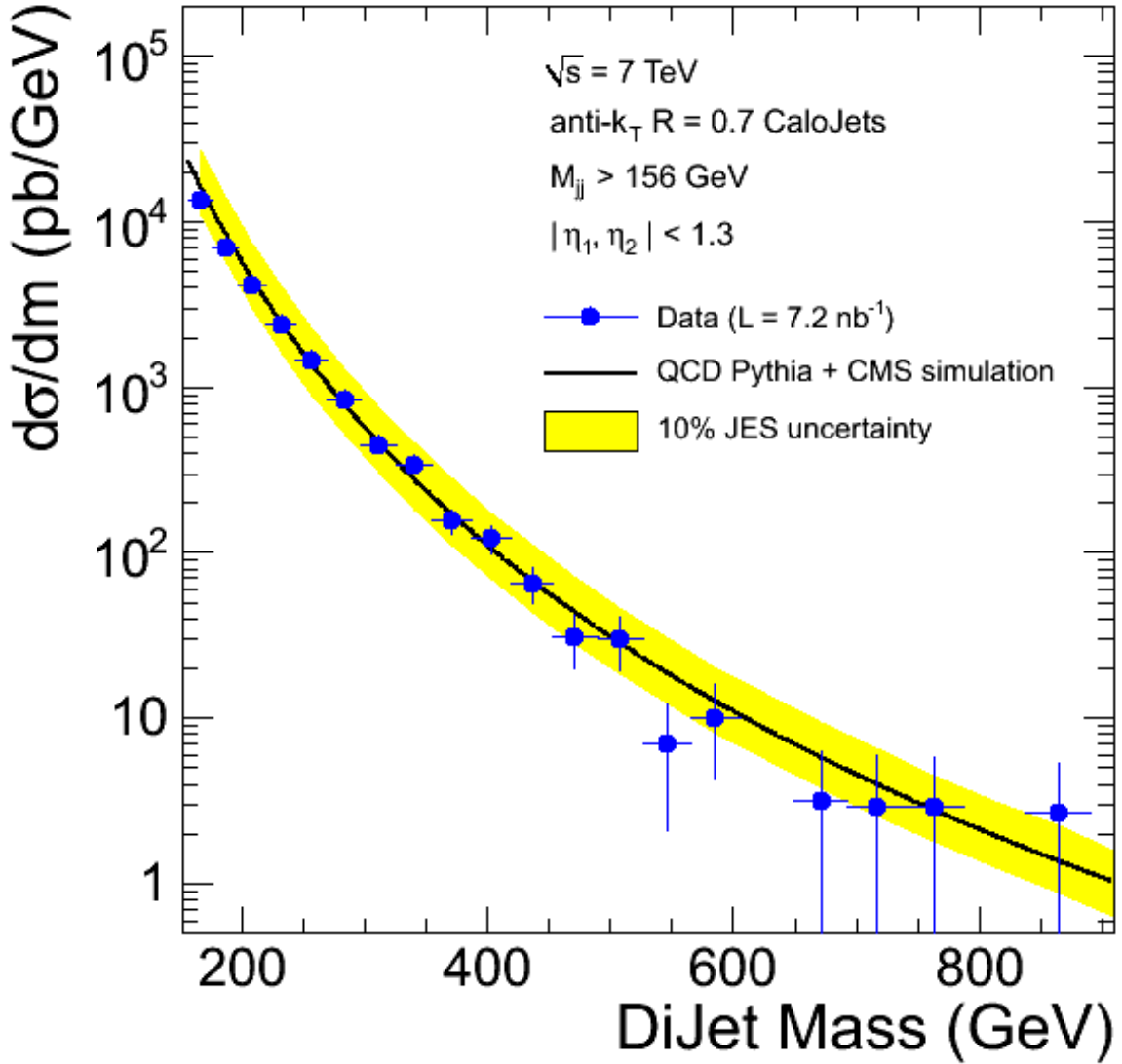

Figure 4: The differential dijet mass spectrum data (points) is compared to a QCD MC prediction (histogram). The quantity plotted is events divided by the bin width, and QCD is normalized to have the same number of events as the data.

Event displays of the ten highest mass dijet events are shown in Appendix B. They all look like good dijet events, with collimated calorimeter energy deposits and associated tracks. The highest dijet mass observed is 764 GeV.

2.5 Dijet Mass Spectrum and Fit

Fig. 5 shows the dijet mass spectrum in the form of an observeed differential cross section as a function of dijet mass.
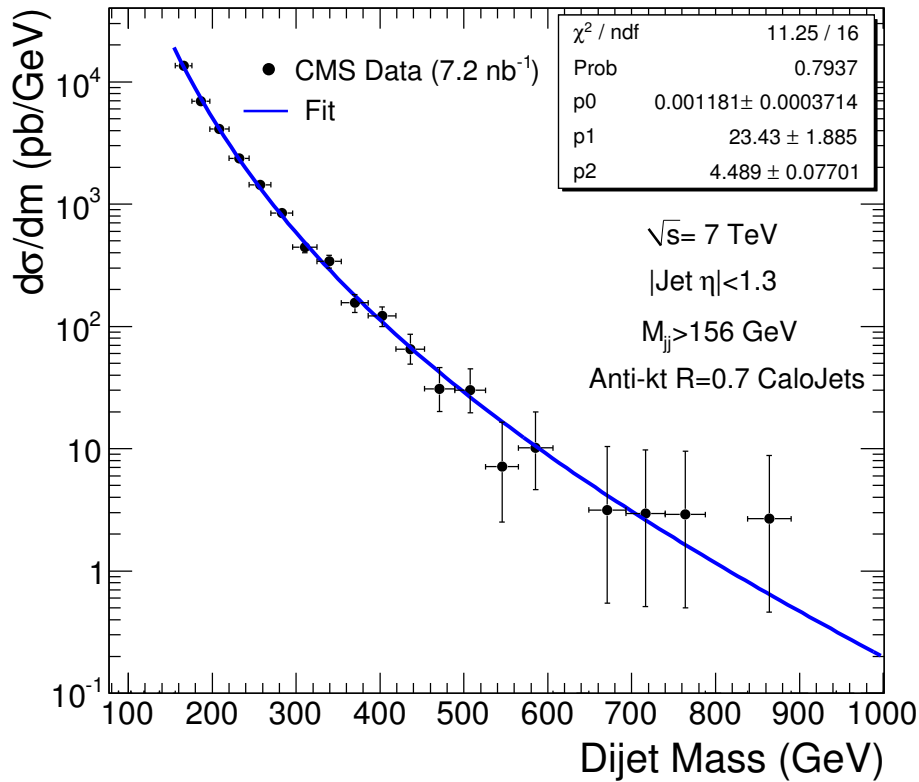

Figure 5: The dijet mass distribution (points) compared to a smooth background fit (solid curve).

The differential cross section is formed using Eq. 2.

$$\frac{d\sigma}{dm} = \frac{1}{\int L dt} \frac{N_i}{\Delta m_i} \tag{2}$$

which includes the integrated luminosity $\int L dt$ but is otherwise the same as eq. 1.

We model the background to a dijet resonance coming from standard model dijet production using a simple parameterization. Our first test for whether there is a bump or other local effect in the data is to simply see if we can get a good fit to a smooth parameterization. Fig. 5 aso shows the parameterization fitted to the data. We get a χ^2 of 3.5 for 12 degrees of freedom for the fit. The paramterization chosen for this data sample was a simple power law with two free parameters in equation 3.

$$\frac{d\sigma}{dm} = \frac{P_0}{m^{P_1}} \tag{3}$$

Fig 6 shows the fractional differences between data and the fit function, (data-fit)/fit, which show no indication of any peaks above the background fit. In the fractional difference plot the error bars are in units of the fit in the bin. Fig. 6 show the pulls, defined as *(Data-Fit)/Error*, which are consistent with statistical fluctuations and are oscillating around zero. In the pulls plot the error bars are always exatly 1, because they are in units of the error in the bin.
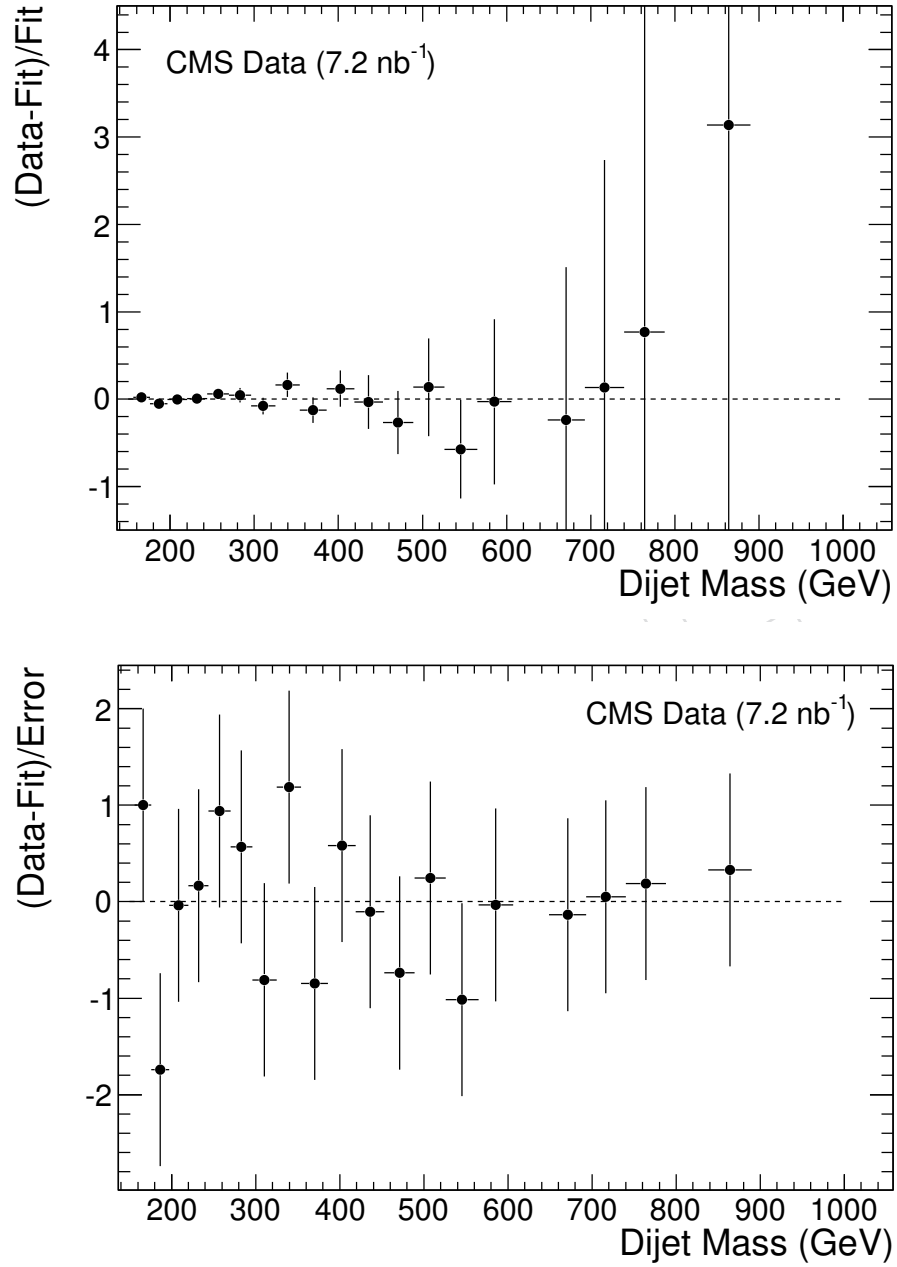
Figure 6: *Top*) The fractional difference between the dijet mass distribution (points) and a smooth background fit as a function of dijet mass. *Bottom*) The pulls distribution (Data-Fit)/Error as a function of dijet mass.

3   Search for Dijet Resonance

3.1   The Signal: Dijet Resonance

The process of $q* \to qg$, $G \to q\bar{q}$ and $G \to gg$ were produced using PYTHIA+CMS simulation at three different masses of 0.7 TeV, 1.2 TeV and 2 TeV. In Fig. 7, we present the resonance shapes which come the process of $q* \to qg$, $G \to q\bar{q}$ and $G \to gg$ at three different masses of 1.2 TeV. Because of different detector responce, ISR and FSR, the resonance shapes are different. The width of dijet resonances increases with number of gluon because gluons emit more radiation than quarks. The low mass tail at resonance shape comes from FSR (Final State Radiation) and high mass tail comes from ISR (Initial State Radiation).
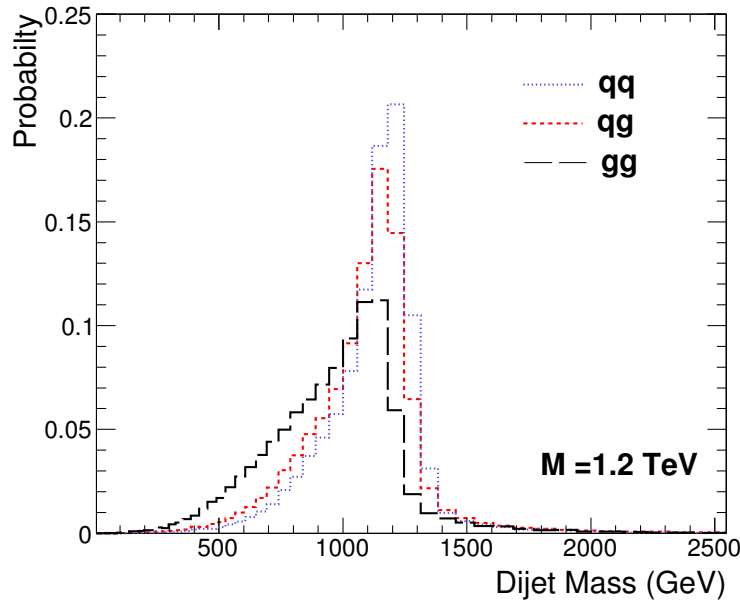

Figure 7: Dijet mass distribution for $q\bar{q}$ (qq), qg and gg resonances of mass at 1.2 TeV.

The resonance shape in intermediate steps between generated resonance masses are obtained using interpolation technique. First, we defined a new parameter as $x = \frac{M_{jj}}{M_{Res}}$ where M_{jj} is dijet mass and M_{Res} is resonance mass. More information can be found in **??**. Fig. 8 shows the simulated signal of excited quark. It can be seen clearly that interpolation technique generates resonable resonance shape and we use these resonance shape to calculate cross section upper limit at any resonance mass.

Fig. 9 shows the differential cross section of excited quark signals as a function of dijet mass with background fit. CMS data based on 7.2 nb^{-1} is compared to the smooth background fit and to simulated resonance signals in Fig. 10.

3.2   Setting Cross Section Upper Limits

Bayesian technique based on binned likelihood is used to calculate the limits on new particle production. The likelihood as a function of a constant can be written as:

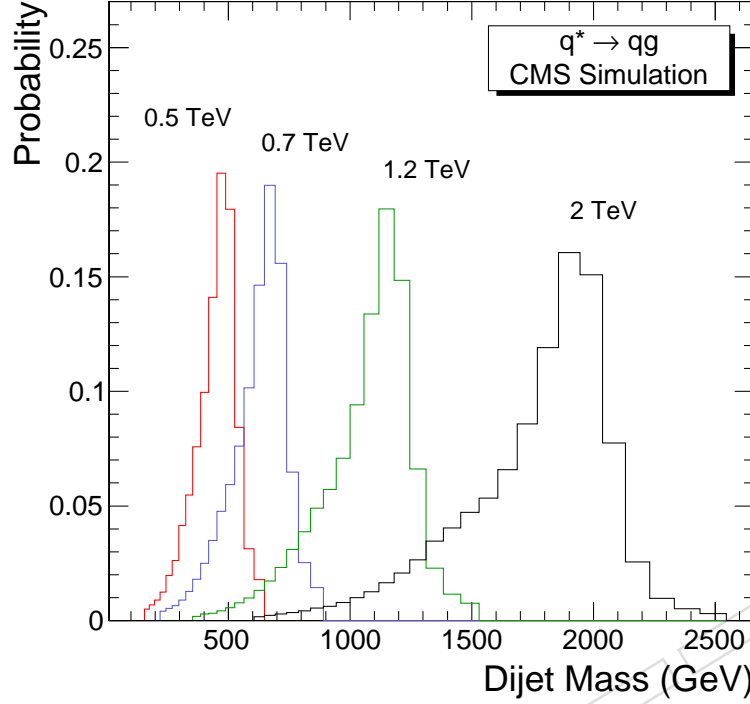$$L = \prod_i \frac{\mu_i^{n_i} e^{-\mu_i}}{n_i!} \tag{4}$$

Figure 8: Resonance shapes at various resonance masses using interpolation technique.

where

$$\mu_i = \alpha N_i(S) + N_i(B). \tag{5}$$

n_i is measured number of events in the $i - th$ dijet mass bin, $N_i(S)$ is number of events from signal in the $i - th$ dijet mass bin, α is a constant to multiply the signal and $N_i(B)$ is number of expected events from background in the $i - th$ dijet mass bin. We consider that QCD background is fixed to the best $Signal + QCD$ fit to data point and it gives the expected number of background event in the $i - th$ dijet mass bin,$N_i(B)$. The number of signal in the $i - th$ dijet mass bin,$N_i(S)$,comes from developed interpolation technique. The signal range is chosen from $0.3 \cdot M_{Res}$ to $1.3 \cdot M_{Res}$ since high and low mass tail is affectively lost in QCD background. Then we plot likelihood distribution as a function of signal cross section for resonances with mass from $0.5 TeV$ to $1.5 TeV$ in $0.1 TeV$ steps, and the 95% confidence level upper limit is calculated as follows;

$$\frac{\int_0^{\sigma_{95}} L(\sigma)d\sigma}{\int_0^{\infty} L(\sigma)d\sigma} = 0.95 \tag{6}$$

In Fig. 11, Likelihood distribution at 0.7 GeV resonance masses for qg resonances are illustrated. The likelihood distributions for resonance mass from 0.5 TeV to 1.5 TeV in 0.1 TeV step can be seen in Appendix X.

We present 95% CL upper limit on Dijet resonance cross section in Fig. 12. Quark-gluon and quark-quark resonances are shown separately. Difference is small between different parton
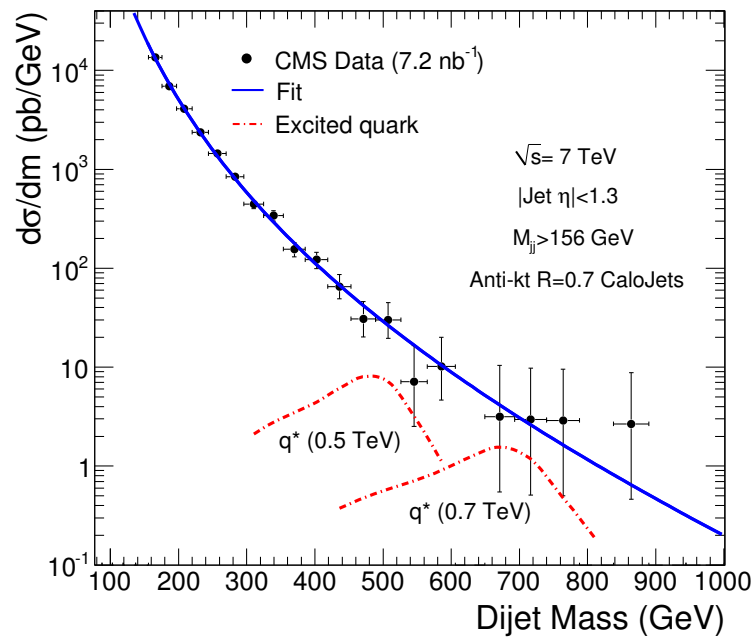
Figure 9: The dijet mass distribution (points) compared to a simulation of excited quarks signals in the CMS detector (dashed red curves).
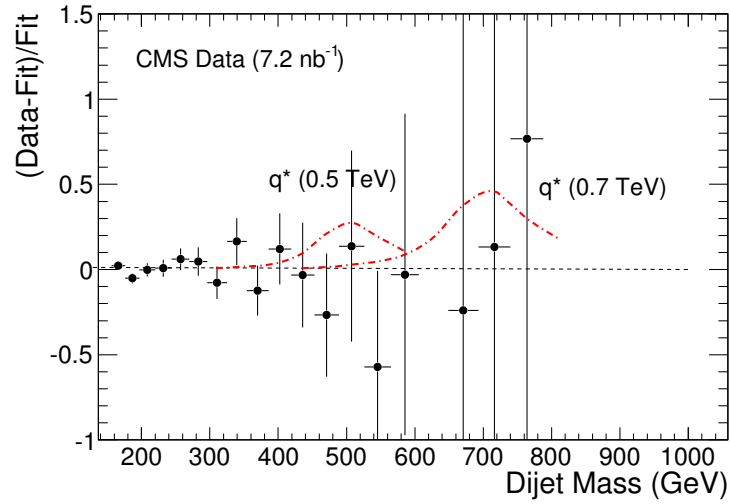
180 pair resonances.

Figure 10: The fractional difference between the dijet mass distribution (points) and a smooth background fit (solid line) is compared to simulations of excited quark signals in the CMS detector (dashed red curves).
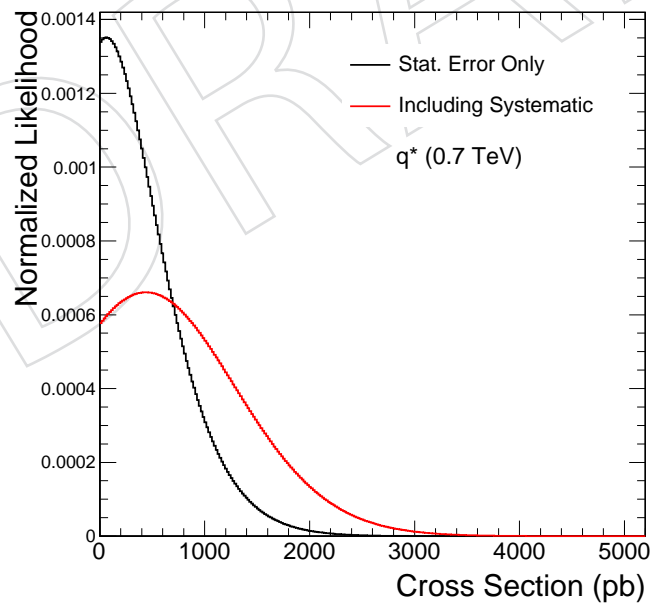

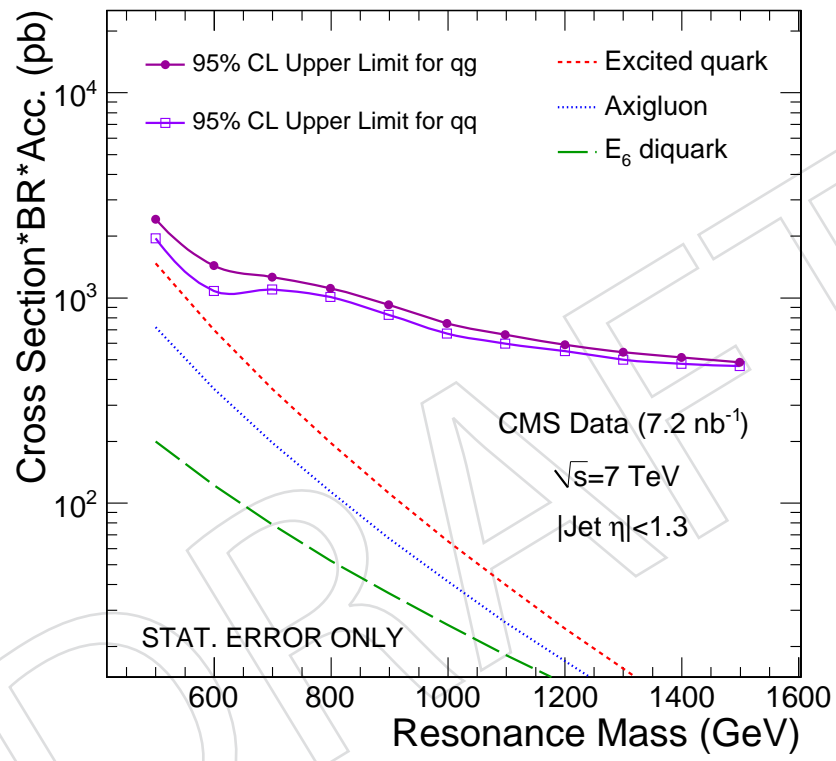Figure 11: Likelihood Distribution with statistical error only.

Figure 12: Dijet resonance sensitivity for 7.2 nb^{-1} CMS data. 95% C.L. is compared to the cross section for various resonance models. This sensitivity contains statistical error only.

4 Systematic Uncertainties

The source of systematic uncertainties are considered as following:

- Jet Energy Scale (JES)
- Jet Energy Resolution (JER)
- Choise of Background Parametrization
- Luminosity

Jet Energy Scale (JES): The uncertainty on JES is basically relatively error between simulation and real data. We assume that the uncertainty on JES is roughly $\pm 10\%$ and the signal is shifted as 10% at startup. It gives more background and finding resonance signal is harder.
The left plot in Fig. 13 shows smooth cross section limit without systematics and with systematics on JES uncertainty for qg resonance. To get smooth cross section limit curve, expected events from background, $N_i(B)$, which is smooth and comes from fit function are considered as measurement number of events, n_i, in the $i-th$ dijet mass bin. Fractional change between smooth limits are illustrated separately at right plot of Fig. 13. The uncertainty on JES varies roughly from 50% at 0.5 *TeV* to 10% at 1.5 *TeV*. Since there is no data point beyond 0.8 *TeV* fractional uncertainty on JES systematic is low after 0.8 *TeV*.

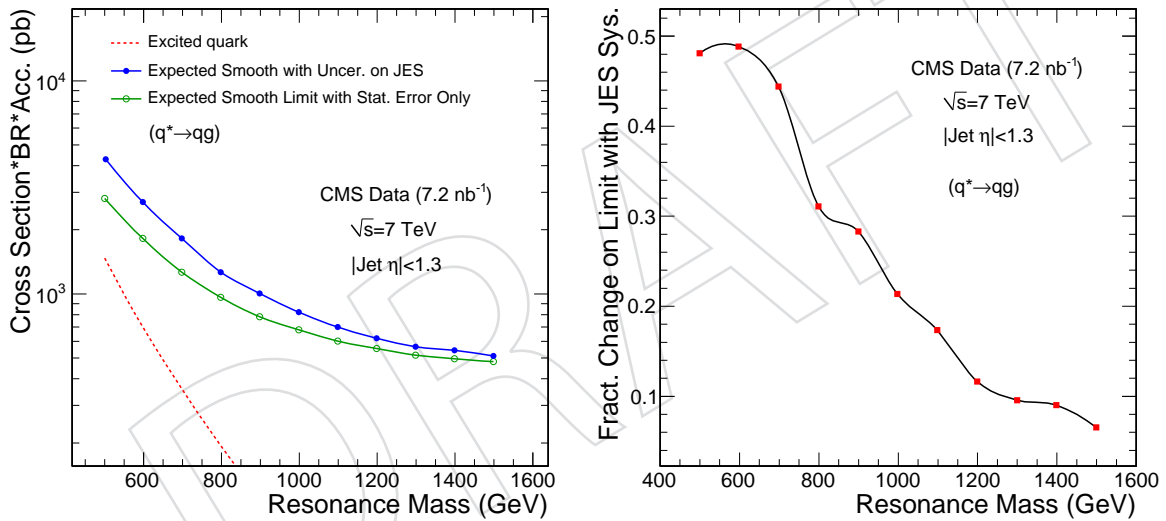Figure 13: *Left plot*: Comparison of smoothed cross section limit without systematics and with systematic on JES uncertainty. *Right plot*:Fractional change on limit with JES systematic uncertainty.

Jet Energy Resolution (JER): We assume that the uncertainty on JER is roughly $\pm 10\%$ and the signal is being smeared with a gausian that increasing core resolution by 10%. A comparison of resonace shapes are shown in Fig.14 ...

Dijet mass core resolution of the resonace signal as a function of resonance mass is illustrated in Fig. 15. The resolution is calculated as *Sigma/Mean* which are obtained from gaussian fit of dijet mass distribution.

The fractional change on Limit with JER systematic is illustared in Fig. 16 . Effect of resolution uncertainty on limit is small.
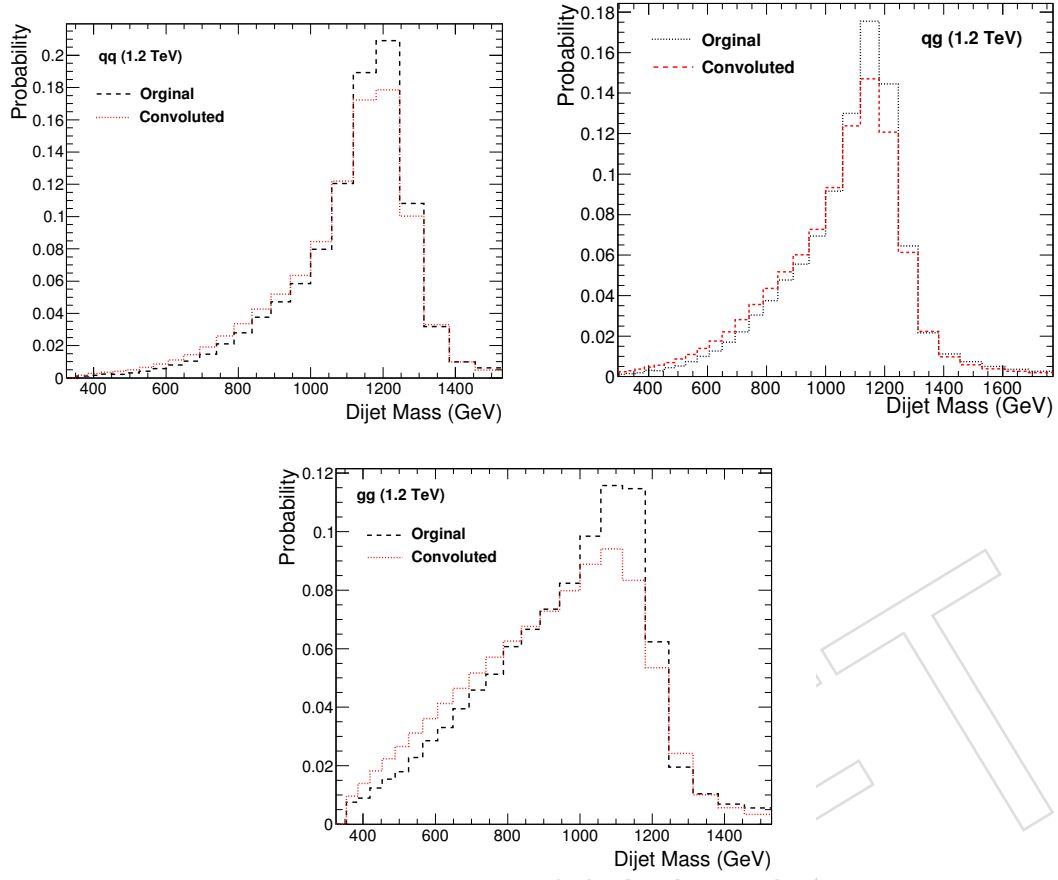
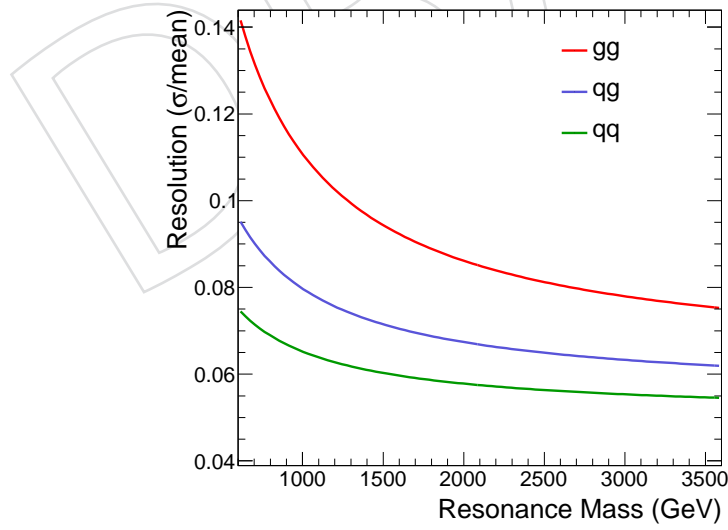Figure 14: Resonance shape comparison after convolution.

Figure 15: The dijet mass resolution as a function of resonance mass.

Background Parametrization Systematic: We considered the others functional forms with 2 and 4 parameters to parameterize the QCD background.
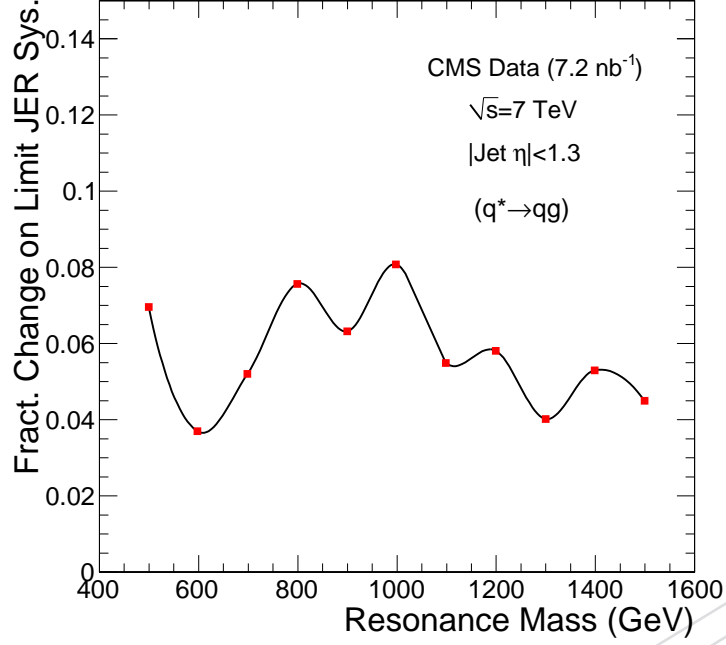
Figure 16: Fractional change on limit with JER systematic uncertainty.

$$\frac{d\sigma}{dm} = p_0 \frac{(1-X)^{p_1}}{X^{p_2}} \tag{7}$$

$$\frac{d\sigma}{dm} = \frac{P_0}{m_1^P} \tag{8}$$

where $X = \frac{m_{jj}}{\sqrt{s}}$. Fig. 17 show comparison of fits with the data points. We found the 2 parameter form gaves the largest fractional change and we used it for Background Parametrization Systematic.

Luminosity: We assumed the uncertainty on luminosity about 10% at startup.

We determine 1σ change for each systematic uncertainty in signal that we can discovery or exclude. To find total total systematics, we add the these 1σ changes as quadrature. The individual and total systematic uncertainties as a function of resonance mass are illustrated in Fig. 18. Absolute uncertainty in each resonance mass is calculated as total systematics uncertainty multiply by upper cross section limit.

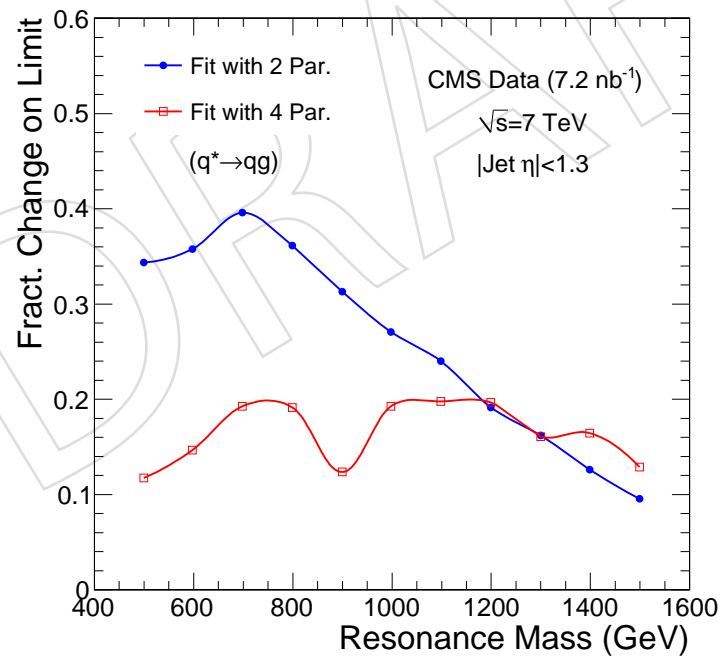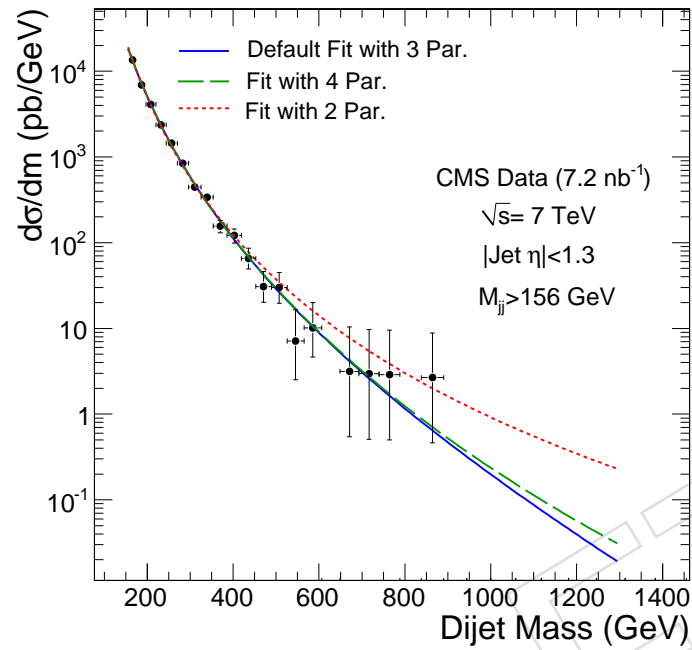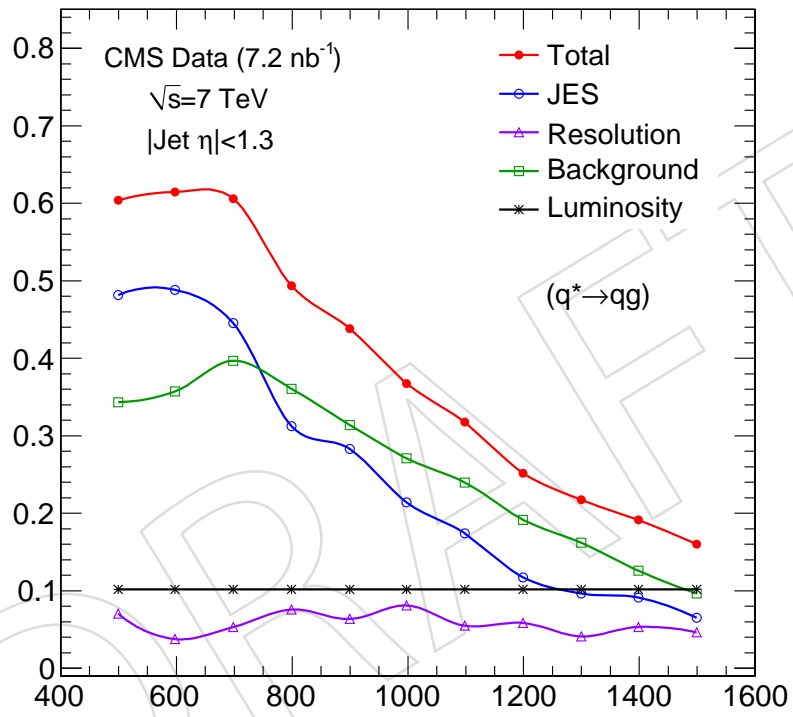The same effect is observed for $q\bar{q}$ (or qq) resonances.

Figure 17:

Figure 18: Fractional systematic uncertainties on signal cross section.

5 Results

I convolute likelihood distribution with gaussian for each resonance mass. The width of gaussian is taken as absolute uncertainty in each resonance mass. The equation of convolution is taken as following

$$L(\check{\sigma}) = \int_0^\infty L(\sigma)G(\sigma)d\sigma \tag{9}$$

Likelihood distributions with systematic uncertainties is shown Fig. 19. Total likelihood includingsystematics is broader and gives higher upper limit.
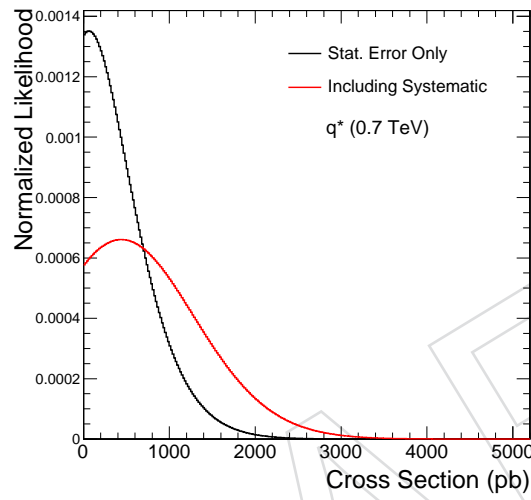

Figure 19: Likelihood distribution with %95 C.L. cross section limit at 0.7 TeV excited quark resonance masses including systematics. Black line is %95 C.L. cross section limit with statistical error only. Red line shows %95 C.L. cross section limit with including systematics.

95% CL Upper limit with Stat. Error. Only and Including Sys. Uncertainties are shown separately in Fig. 20. The effects of systematics is presented Fig. 20. Cross section limits increase by about 50% - 10% with systematics uncertainties.

Dijet resonance sensitivity for quark-gluon and quark-quark resonances including systematic uncertainties is illustrated in Fig. 21.
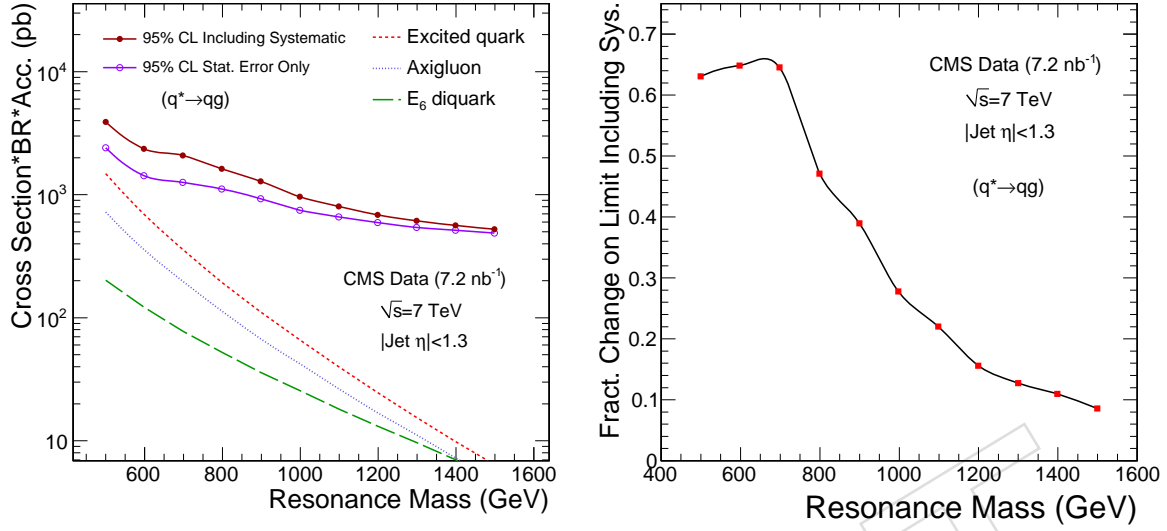
Figure 20: Fractional change on limit with including systematics.

Mass	95% C.L. $\sigma \cdot B$ (pb)	
(*TeV*)	Stat. Error Only	Including Systematic Uncer.
0.5	2402	3915
0.6	1416	2333
0.7	1254	2061
0.8	1101	1620
0.9	923	1281
1.0	746	953
1.1	654	797
1.2	584	675
1.3	542	610
1.4	507	562
1.5	481	522

Table 3: As a function of excited quark mass we list our 95% C.L. upper limit on cross section times branching ratio for narrow resonances of excited quark decaying to dijets

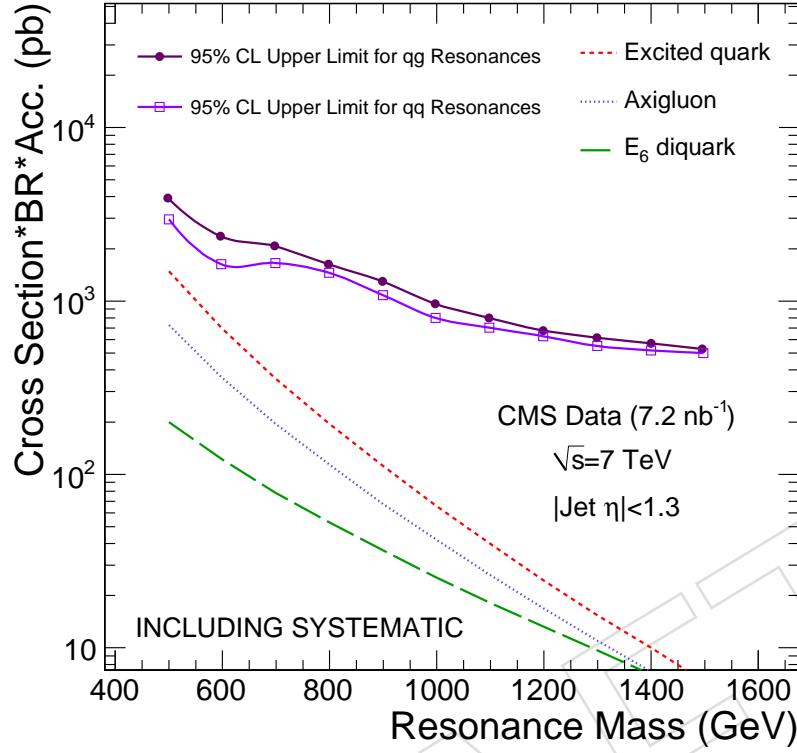Figure 21: Dijet resonance sensitivity including systematic uncertainties.

Mass	95% C.L. $\sigma \cdot B$ (pb)	
(*TeV*)	quark-quark	quark-gluon
0.5	2912	3915
0.6	1599	2333
0.7	1632	2061
0.8	1440	1620
0.9	1066	1281
1.0	794	953
1.1	689	797
1.2	617	675
1.3	541	610
1.4	513	562
1.5	495	522

Table 4: As a function of resonance mass we list our 95% C.L. upper limit on cross section times branching ratio for narrow resonances of quark-quark and quark-gluon resonances including systematic uncertainties.

228 **6   Conclusions**

A   Resonance Model Cross Sections

Mass (GeV)	q^* (pb)	A or C (pb)	D (pb)	Z' (pb)	W' (pb)	G (pb)
500.0	0.1472E+04	0.7155E+03	0.1993E+03	0.1884E+02	0.3248E+02	0.4516E+02
600.0	0.6940E+03	0.3584E+03	0.1210E+03	0.9749E+01	0.1729E+02	0.1816E+02
700.0	0.3562E+03	0.1950E+03	0.7789E+02	0.5435E+01	0.9874E+01	0.8186E+01
800.0	0.1942E+03	0.1123E+03	0.5219E+02	0.3191E+01	0.5913E+01	0.4016E+01
900.0	0.1107E+03	0.6731E+02	0.3597E+02	0.1944E+01	0.3663E+01	0.2101E+01
1000.0	0.6529E+02	0.4158E+02	0.2531E+02	0.1218E+01	0.2325E+01	0.1156E+01
1100.0	0.3956E+02	0.2627E+02	0.1808E+02	0.7793E+00	0.1504E+01	0.6618E+00
1200.0	0.2449E+02	0.1689E+02	0.1306E+02	0.5069E+00	0.9858E+00	0.3913E+00
1300.0	0.1542E+02	0.1101E+02	0.9522E+01	0.3339E+00	0.6528E+00	0.2374E+00
1400.0	0.9852E+01	0.7258E+01	0.6986E+01	0.2223E+00	0.4356E+00	0.1471E+00
1500.0	0.6370E+01	0.4826E+01	0.5151E+01	0.1492E+00	0.2922E+00	0.9273E-01
1600.0	0.4159E+01	0.3231E+01	0.3811E+01	0.1008E+00	0.1967E+00	0.5929E-01
1700.0	0.2738E+01	0.2176E+01	0.2827E+01	0.6847E-01	0.1327E+00	0.3835E-01
1800.0	0.1816E+01	0.1472E+01	0.2100E+01	0.4670E-01	0.8961E-01	0.2505E-01
1900.0	0.1211E+01	0.9988E+00	0.1562E+01	0.3196E-01	0.6049E-01	0.1648E-01
2000.0	0.8122E+00	0.6795E+00	0.1161E+01	0.2192E-01	0.4079E-01	0.1092E-01
2100.0	0.5468E+00	0.4631E+00	0.8633E+00	0.1506E-01	0.2745E-01	0.7264E-02
2200.0	0.3694E+00	0.3160E+00	0.6411E+00	0.1035E-01	0.1842E-01	0.4852E-02
2300.0	0.2502E+00	0.2156E+00	0.4753E+00	0.7118E-02	0.1231E-01	0.3249E-02
2400.0	0.1698E+00	0.1470E+00	0.3517E+00	0.4891E-02	0.8196E-02	0.2180E-02
2500.0	0.1154E+00	0.1002E+00	0.2596E+00	0.3356E-02	0.5428E-02	0.1463E-02
2600.0	0.7850E-01	0.6811E-01	0.1910E+00	0.2298E-02	0.3574E-02	0.9819E-03
2700.0	0.5342E-01	0.4619E-01	0.1401E+00	0.1569E-02	0.2339E-02	0.6582E-03
2800.0	0.3635E-01	0.3123E-01	0.1023E+00	0.1067E-02	0.1520E-02	0.4404E-03
2900.0	0.2472E-01	0.2103E-01	0.7444E-01	0.7232E-03	0.9803E-03	0.2939E-03
3000.0	0.1679E-01	0.1410E-01	0.5389E-01	0.4876E-03	0.6272E-03	0.1954E-03
3100.0	0.1139E-01	0.9398E-02	0.3881E-01	0.3269E-03	0.3978E-03	0.1294E-03
3200.0	0.7715E-02	0.6227E-02	0.2779E-01	0.2177E-03	0.2500E-03	0.8518E-04
3300.0	0.5214E-02	0.4098E-02	0.1977E-01	0.1440E-03	0.1557E-03	0.5575E-04
3400.0	0.3515E-02	0.2676E-02	0.1398E-01	0.9445E-04	0.9596E-04	0.3623E-04
3500.0	0.2364E-02	0.1733E-02	0.9809E-02	0.6141E-04	0.5858E-04	0.2336E-04
3600.0	0.1585E-02	0.1111E-02	0.6830E-02	0.3955E-04	0.3541E-04	0.1493E-04
3700.0	0.1059E-02	0.7055E-03	0.4716E-02	0.2520E-04	0.2119E-04	0.9452E-05
3800.0	0.7059E-03	0.4430E-03	0.3227E-02	0.1587E-04	0.1257E-04	0.5920E-05
3900.0	0.4687E-03	0.2749E-03	0.2186E-02	0.9880E-05	0.7398E-05	0.3666E-05
4000.0	0.3102E-03	0.1684E-03	0.1466E-02	0.6069E-05	0.4321E-05	0.2243E-05
4100.0	0.2046E-03	0.1018E-03	0.9714E-03	0.3679E-05	0.2510E-05	0.1354E-05

Table 5: Cross section for dijet resonances in pp collisions at $\sqrt{s} = 7$ TeV with jet pseudorapidity $|\eta| < 1.3$. The models are Excited Quark (q*), Axigluon or Coloron (A or C), E_6 diquark (D), Z', W' and Randall-Sundrum Graviton (G).Lowest order calculation described previously [3]
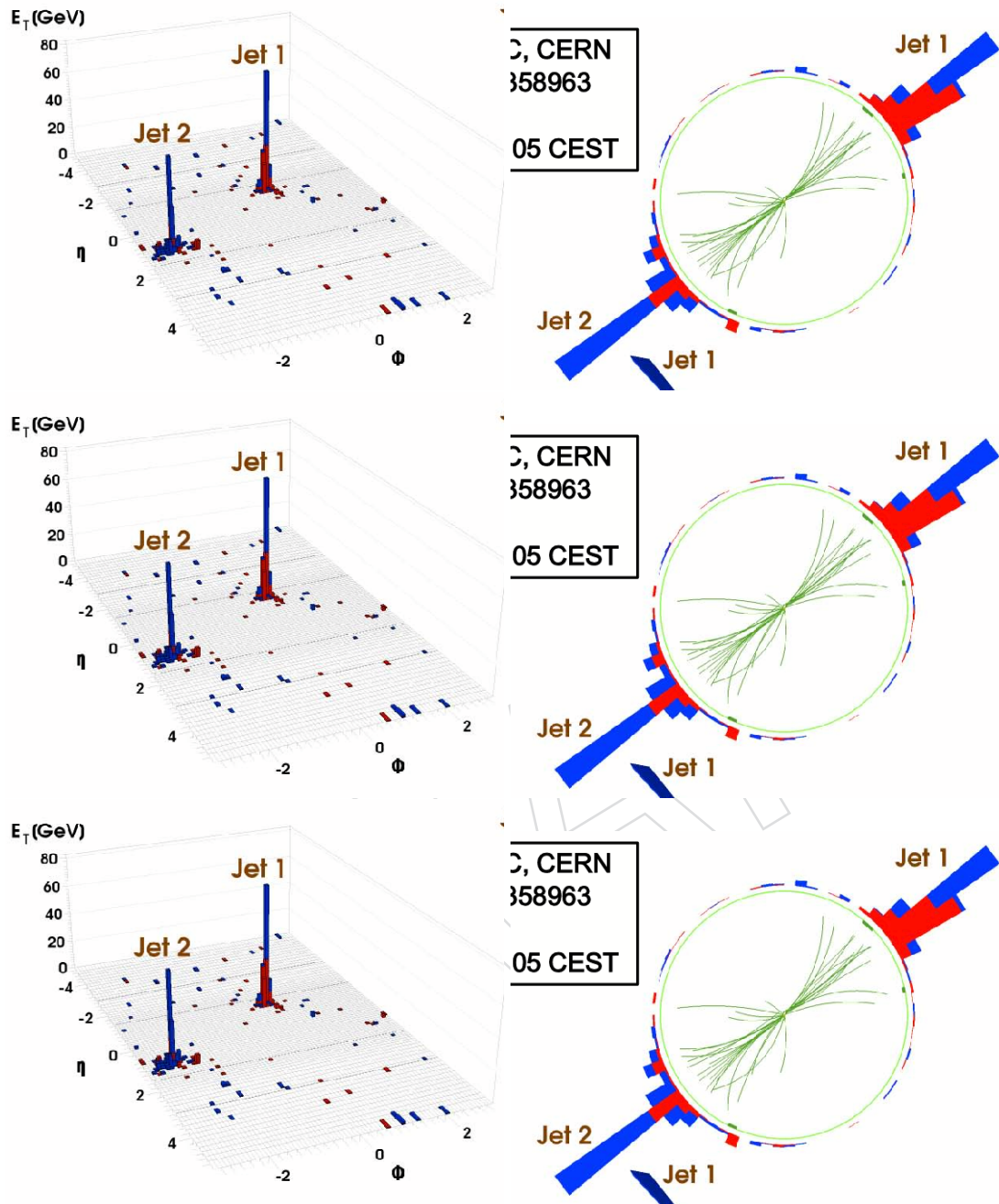
B Event Displays of High Mass Dijet Events

Figure 22: Lego (left) and $\rho - \phi$ (right) displays of the 1st to 3rd Highest Masss Dijet Events
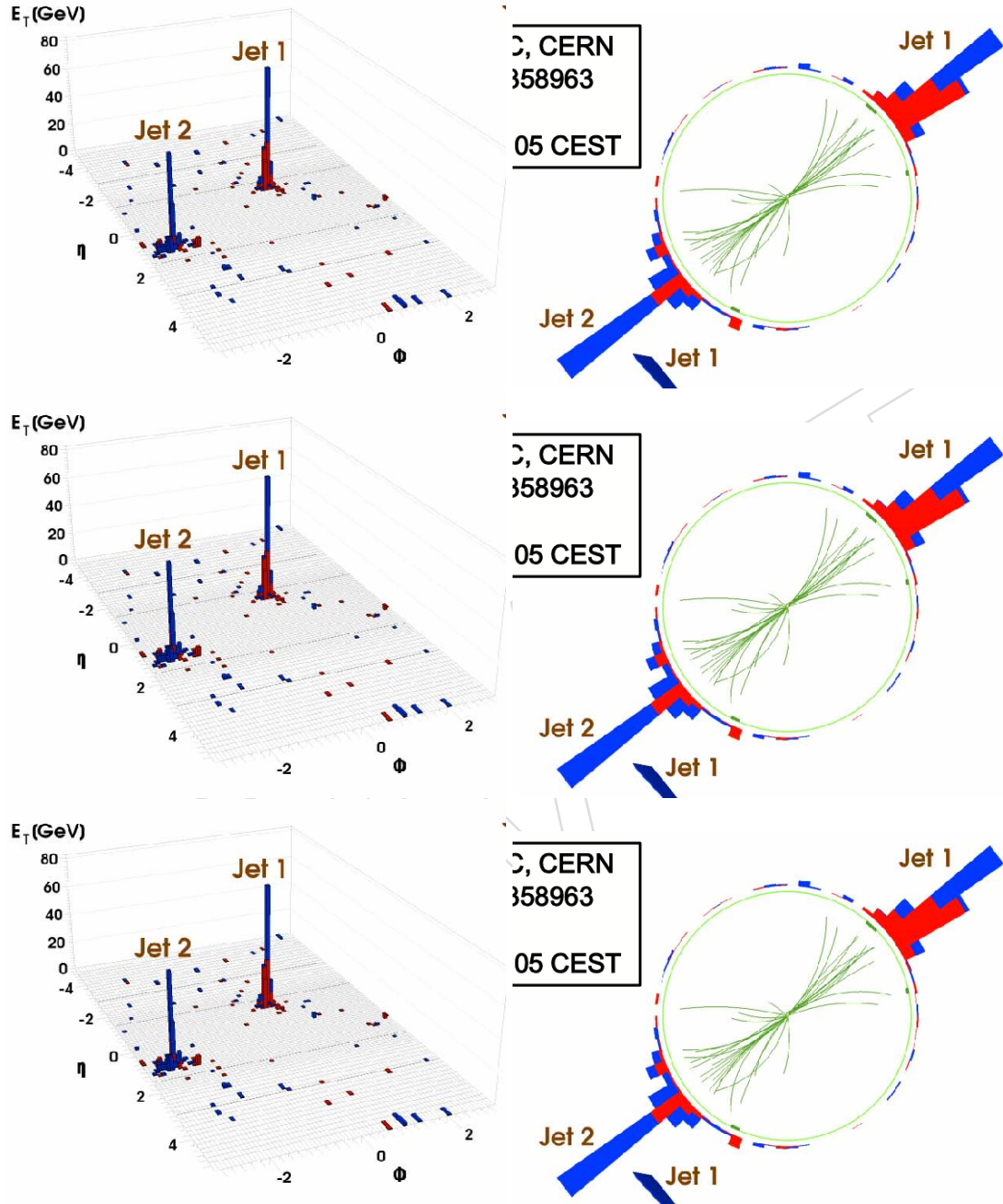
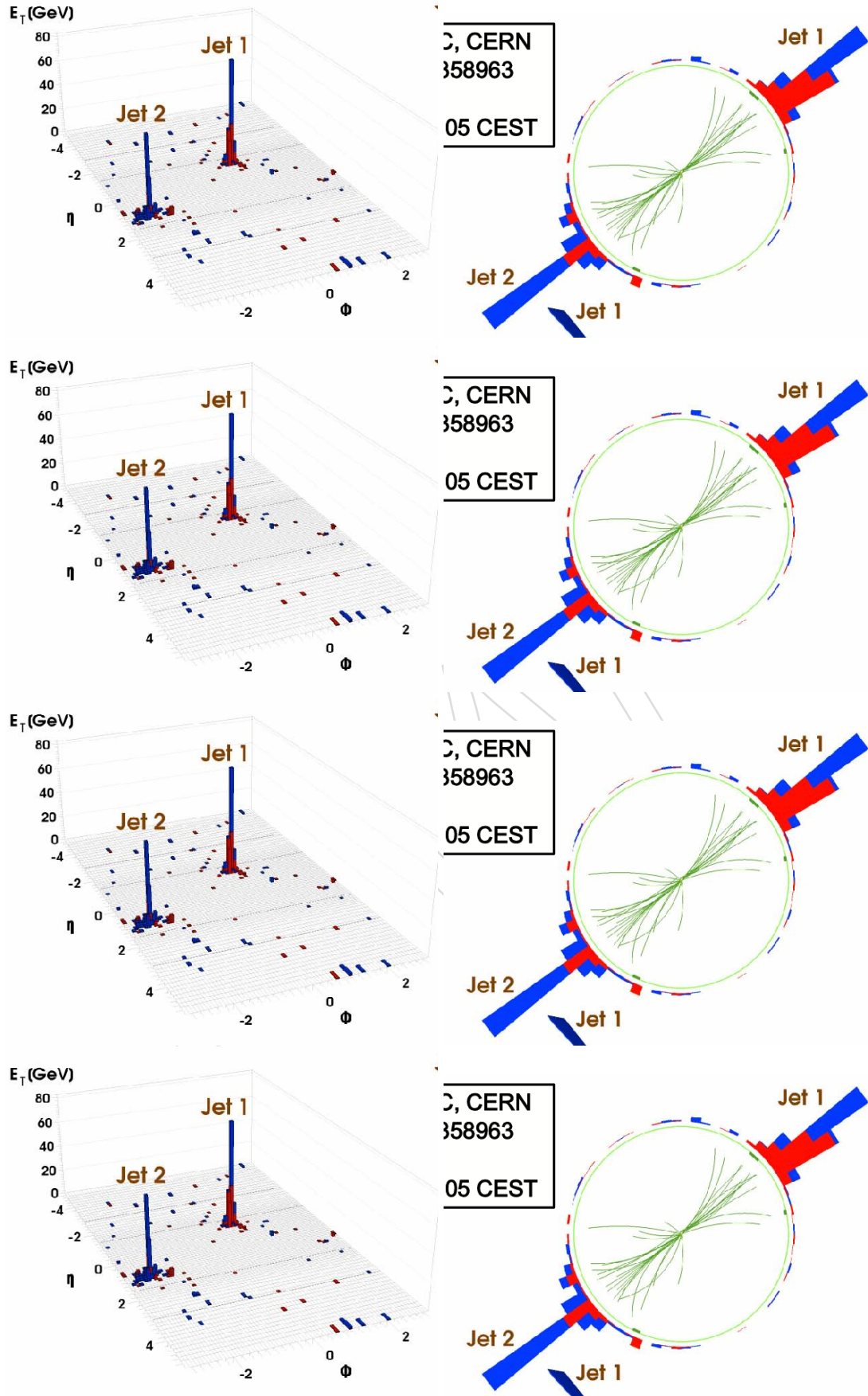Figure 23: Lego (left) and $\rho - \phi$ (right) displays of the 4th to 6th Highest Masss Dijet Events

Figure 24: Lego (left) and $\rho - \phi$ (right) displays of the 7th to 10th Highest Masss Dijet Events

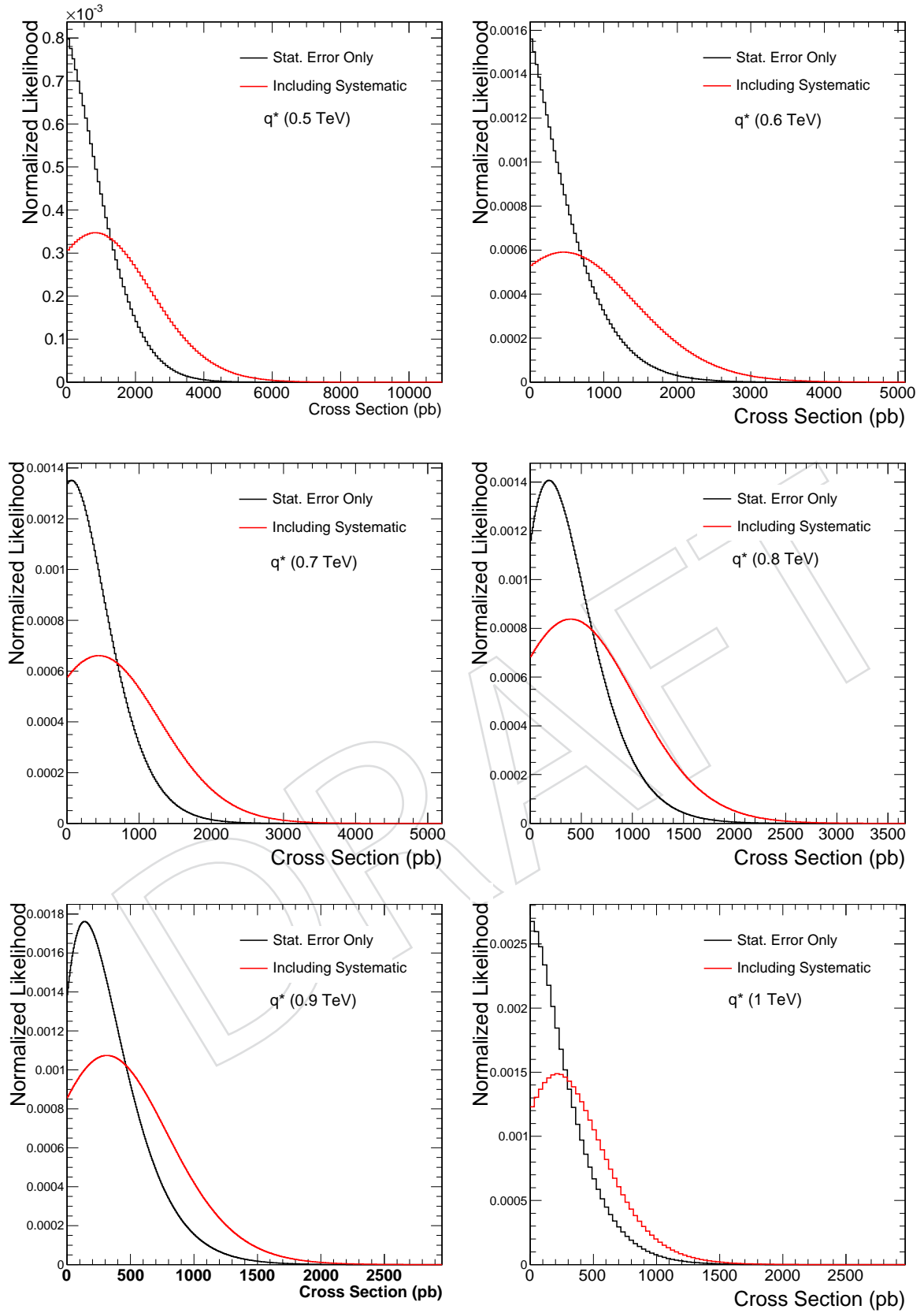₂₃₁ # C Likelihood Distributions

Figure 25: Likelihood distribution with %95 C.L. cross section limit at various excited quark resonance masses including systematics. Black line is %95 C.L. cross section limit with statistical error only. Red line shows %95 C.L. cross section limit with including systematics.
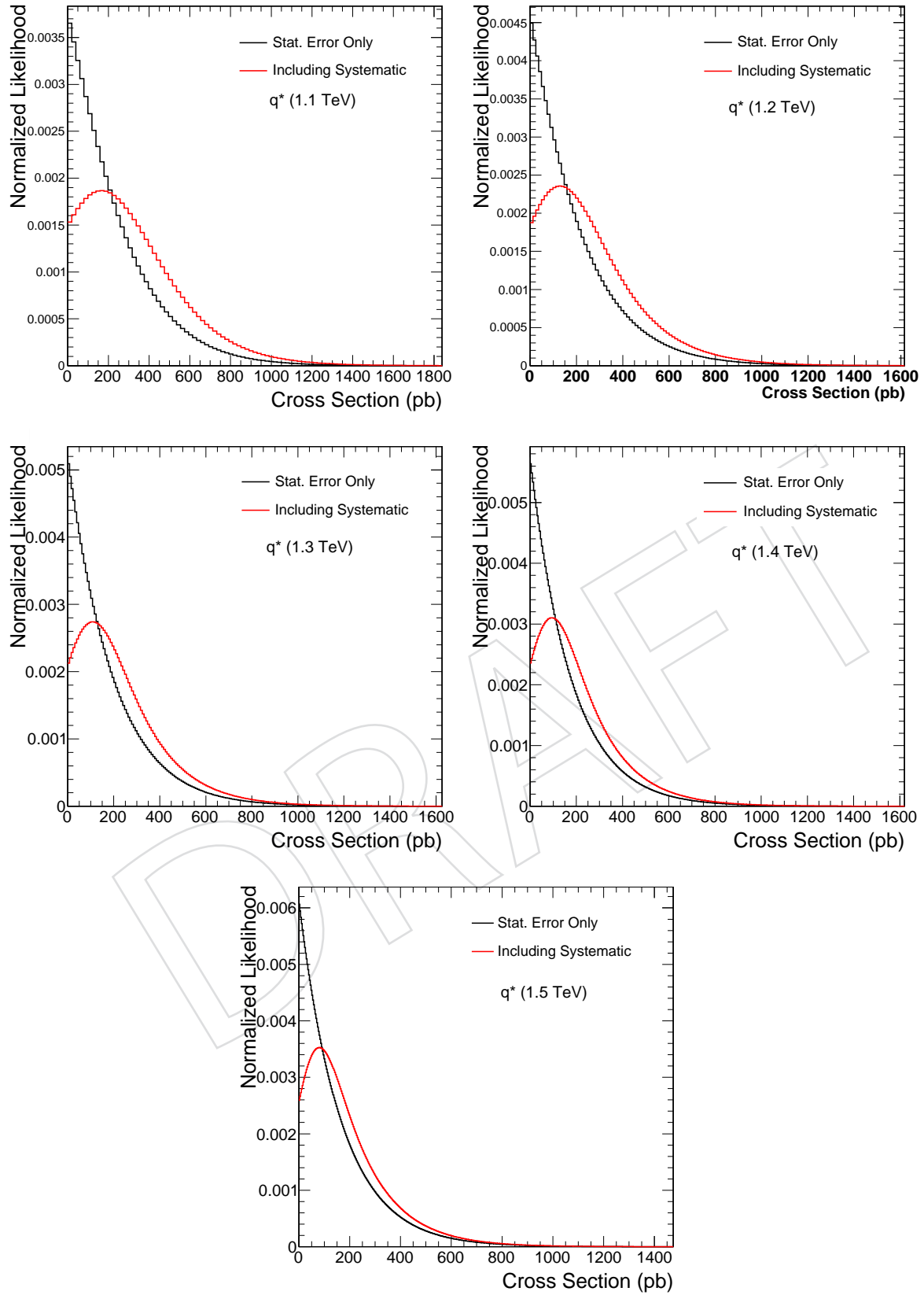
Figure 26: Likelihood distribution with %95 C.L. cross section limit at various excited quark resonance masses including systematics. Black line is %95 C.L. cross section limit with statistical error only. Red line shows %95 C.L. cross section limit with including systematics.

References

[1] S. Ozturk, C. Jeong, S. Lee et al., "Plans to Search for New Particles Decaying to Dijets in pp Collisions at sqrt(s)=10 TeV", *CMS AN-* **2009/070 HYPERLINK** (2009).

[2] C. Jeong, S. Lee, I. Volobuev et al., "Dijet Resonance Shapes for sqrt(s)=10 TeV", *CMS AN-* **2009/145 HYPERLINK** (2009).

[3] K. Gumus, N. Akcshurin, S. Esen et al., "CMS Senitivity to Dijet Resonances", *CMS Note* **2006/070 HYPERLINK** (2006).

[4] U. Baur, I. Hinchliffe, and D. Zeppenfeld, "EXCITED QUARK PRODUCTION AT HADRON COLLIDERS", *Int. J. Mod. Phys.* **A2** (1987) 1285.

[5] J. Bagger, C. Schmidt, and S. King, "AXIGLUON PRODUCTION IN HADRONIC COLLISIONS", *Phys. Rev.* **D37** (1988) 1188.

[6] R. S. Chivukula, A. G. Cohen, and E. H. Simmons, "New Strong Interactons at the Tevatron ?", *Phys. Lett.* **B380** (1996) 92–98, `arXiv:hep-ph/9603311`.

[7] J. L. Hewett and T. G. Rizzo, "LOW-ENERGY PHENOMENOLOGY OF SUPERSTRING INSPIRED E(6) MODELS", *Phys. Rept.* **183** (1989) 193.

[8] L. Randall and R. Sundrum, "Large Mass Hierarchy from a Small Extra Dimension", *Phys. Rev. Lett.* **83** (1999) 3370.

[9] E. Eichten, I. Hinchliffe, K. D. Lane et al., "SUPER COLLIDER PHYSICS", *Rev. Mod. Phys.* **56** (1984) 579–707.

[10] **CDF** Collaboration, T. Aaltonen et al., "Search for new particles decaying into dijets in proton- antiproton collisions at sqrt(s) = 1.96 TeV", *Phys. Rev.* **D79** (2009) 112002, `arXiv:0812.4036.doi:10.1103/PhysRevD.79.112002`.